First-principles structure determination of interface materials: The Ni$_x$InAs nickelides

Georg Schusteritsch,[1,*] Steven P. Hepplestone,[1] and Chris J. Pickard[1,2]

[1]*Department of Physics and Astronomy, University College London, Gower Street, London WC1E 6BT, United Kingdom*
[2]*London Institute for Mathematical Sciences, 35a South Street, Mayfair, London W1K 2XF, United Kingdom*

We present here a first-principles study of the ternary compounds formed by Ni, In, and As, a material of great importance for self-aligned metallic contacts in next-generation InAs-based MOS transistors. The approach we outline is general and can be applied to study the crystal structure and properties of a host of other new interface compounds. Using the *ab initio* random structure searching approach we find the previously unknown low-energy structures of Ni$_x$InAs and assess their stability with respect to the known binary compounds of Ni, In, and As. Guided by experiments, we focus on Ni$_3$InAs and find a rich energy landscape for this stoichiometry. We consider the five lowest-energy structures, with space groups $Pmmn$, $Pbcm$, $P2_1/m$, $Cmcm$, and $R\bar{3}$. The five low-energy structures for Ni$_3$InAs are all found to be metallic and nonmagnetic. By comparison to previously published TEM results we identify the crystal structure observed in experiments to be $Cmcm$ Ni$_3$InAs. We calculate the work function for $Cmcm$ Ni$_3$InAs and, according to the Schottky-Mott model, expect the material to form an Ohmic contact with InAs. We further explicitly consider the interface between $Cmcm$ Ni$_3$InAs and InAs and find it to be Ohmic with an n-type Schottky barrier height of -0.55 eV.

PACS number(s): 71.15.Mb, 61.50.Ah, 68.55.−a, 73.40.Cg

I. INTRODUCTION

Device size scaling is reaching its limits for conventional silicon (Si) complementary metal-oxide semiconductor (CMOS) transistors and new strategies have to be identified for the next generation of transistors [1]. One pathway to break this scaling barrier is in the usage of III-V semiconductors as the channel materials [1–3]. These materials have higher electron mobilities than Si, outstanding frequency response and have been shown to have excellent on/off state switching properties (see Ref. [2] and references therein). Many challenges that relate to the device architecture as a whole, however, still remain and a particularly important issue that needs to be addressed is to identify suitable interface materials that can function as low resistance Ohmic metallic contacts to III-V semiconductors. Finding such new contact materials is imperative for the overall viability of III-V-based transistors and in fact has been identified as one of the grand challenges for logic device scaling by the International Technology Roadmap for Semiconductors (ITRS) [1], the *de facto* strategic master plan set by the semiconductor industry.

In conventional Si CMOS, contacts are usually fabricated through a self-aligned process creating metal silicides through deposition followed by annealing, crucially without the need of lithographic techniques. A similar procedure may be essential for economical mass production of III-V-based transistors with highly scaled dimensions. Among the possible III-V semiconductors, indium arsenide (InAs) has been identified as a particularly beneficial channel material and has been demonstrated in several experimental transistors [4]. It was recently shown that self-aligned silicidelike contacts can be made to InAs using nickel (Ni) to form a ternary Ni$_x$InAs compound [5].

To date, little is known about the ternary compounds Ni, In, and As form. It has been reported in several experimental studies that the ternary compounds are crystalline [5–7] and several studies suggest the stoichiometry to be Ni$_3$InAs [5,6], though some experiments suggest Ni$_2$InAs [8,9] or altogether different stoichiometries [7]. It is also suggested that the phases observed in experiments are metallic [5,6]. To the best of our knowledge, no experimental nor theoretical study has yet uniquely identified the crystal structure of the ternary Ni-In-As compounds, nor are we aware of any in-depth study of its physical properties. Further development of the InAs transistor technology hinges on a better understanding of the properties of contact materials in general and, given the initial experimental successes, of the Ni-In-As nickelide compounds in particular.

In this paper we show how theoretical methods can be used to first identify the crystal structure of the Ni-In-As ternary compounds, study their mechanical and electronic properties, investigate their stability, and assess the electronic properties of the interface they form with InAs. The theoretical strategy outlined here is general and can be applied to a host of other systems. Specifically, we use the *ab initio* random structure searching (AIRSS) approach [10] to find the previously unknown crystal structures of Ni$_x$InAs, for $x = 1$–6. We focus on the five lowest-energy structures of Ni$_3$InAs and by comparison with the limited experimental information available, we identify that the nickelide forms in the orthorhombic $Cmcm$ structure in the experiments reported in Ref. [5], and is a higher-energy metastable state. All low-energy Ni$_3$InAs structures are found to be metallic and nonmagnetic. We further consider the interface between $Cmcm$ Ni$_3$InAs and InAs and find evidence for Ohmic behavior. Our study shows that structure prediction tools in combination with conventional theoretical methods are now at a stage where these can lead to disruptive innovations in many fields of industry.

*g.schusteritsch@ucl.ac.uk

II. COMPUTATIONAL METHOD

AIRSS has previously been successfully applied to predict the crystal structure of bulk materials [11–14], single-point defects [15–17], and interfaces [18]. The approach is fully first-principles and shown to be sufficiently efficient to address ternary systems with large unit cells here. The system sizes we consider are between 4–25 atoms in the unit cell with three different species. All our structure searching calculations as well as the majority of the calculations determining the physical properties were performed using density functional theory (DFT) as implemented in the CASTEP [19] plane-wave code. For finding the crystal structure of Ni_xInAs, we initially search with coarse parameters and soft pseudopotentials and then refine our final structures with stricter parameters and harder pseudopotentials to accurately rank the lowest-energy structures according to their energy and to determine their mechanical and electronic properties. Structural relaxations are performed using the Broyden-Fletcher-Goldfarb-Shanno (BFGS) method. During searching we relax all forces to a magnitude of less than 0.05eV/Å followed by a stricter tolerance of 0.01eV/Å for the final results. For searching we use pseudopotentials that treat the valence electrons for the $3d^8$, $4s^2$ states for Ni, the $4s^2$, $4p^3$ states for As, and the $4d^{10}$, $5s^2$, $5p^1$ states for In. Our final results are calculated using harder core-corrected on-the-fly-generated pseudopotentials that treat the $3d^8$, $4s^2$ states for Ni, the $4s^2$, $4p^3$ states for As, and the $4s^2$, $4p^6$, $4d^{10}$, $5s^2$, $5p^1$ states for In. A plane-wave cut-off energy of 360 eV for searching and 575 eV for the final calculations was chosen to satisfy convergence. We use a Monkhorst-Pack grid density with a maximum distance between two k points of 0.05 Å^{-1} for searching and 0.03 Å^{-1} for the final calculations. The exact XC energy is approximated by the PBEsol generalized gradient approximation [20] unless otherwise stated. We show in Table I the lattice constants, density, bulk modulus, shear modulus, and Young's modulus for InAs and Ni with the respective experimental values for comparison. We find PBEsol to be best suited to describe the structure of both InAs and Ni separately, consistent with Haas *et al.* [21]. To find the Schottky barrier height of the $InAs/Ni_3InAs$ interface, we perform calculations using the VASP [22–24] plane-wave code, using the exact XC energy approximated by the generalized gradient approximation within the PBE framework [33], in combination with calculations using the hybrid Heyd-Scuseria-Ernzerhof functional (HSE06) [26,27]. An energy cutoff of 270 eV

was used unless otherwise stated. For all calculations, PAW potentials with a total valency of 10, 5, and 13 are generated for Ni, In, and As, respectively [23,24].

III. RESULTS AND DISCUSSION

Most experimental realizations of the Ni-In-As ternary nickelides involve growth by diffusion of Ni into InAs. We are therefore primarily interested in Ni-In-As compounds for which In and As are present in equal quantities and search for structures with stoichiometries Ni_xInAs with $x = 1$–6 and between 1–5 formula units (f.u.). We show in Fig. 1 the ternary phase diagram for our ternary compounds and the known binary compounds of Ni, In, and As. We also show
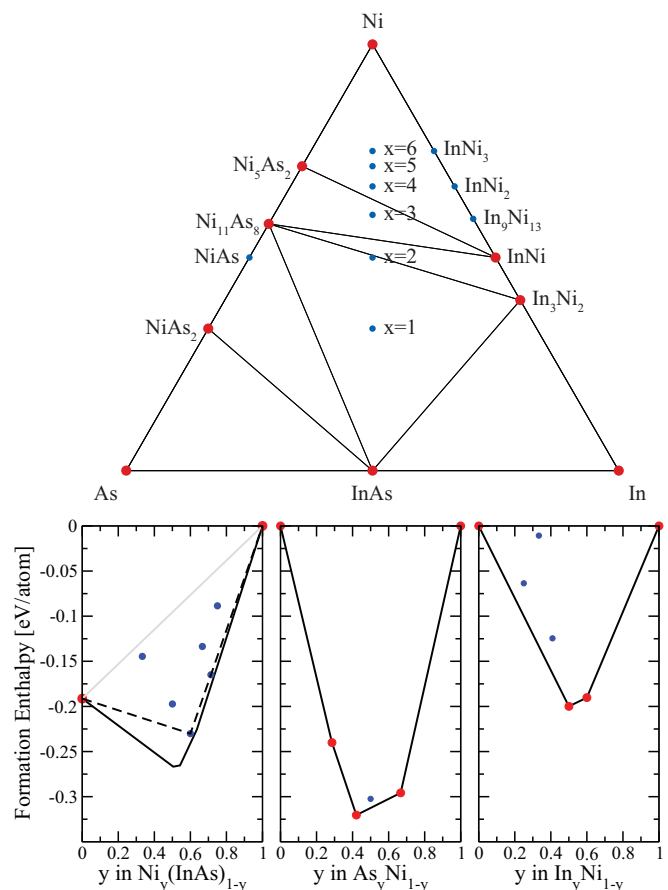

FIG. 1. (Color online) Ternary phase diagram of the Ni-In-As system shown at the top, with slices through the ternary convex hull shown at the bottom. Structures that are found to be stable are shown as red dots, while structures that do not fall onto the convex hull are shown as blue dots. Blue dots labeled $x = 1$–6 indicate the positions of the structures Ni_xInAs on the ternary diagram. The left-hand side, center, and right-hand side plots at the bottom show the slices through the ternary phase diagram along InAs to Ni, As to Ni, and In to Ni, respectively. The slices through the ternary phase diagrams are shown as black solid lines, while the binary convex hull for InAs and Ni is shown as a black dashed line, with the gray line indicating the zero offset to the binary convex hull. Ni_3InAs is found to be stable for the binary system InAs/Ni, while it is marginally unstable by 0.01eV/atom on the ternary convex hull. The ternary phase diagram is based on a plot created using the STOOLS analysis tool set [36].

TABLE I. Lattice constant (a_0), density (ρ), bulk modulus (B), shear modulus (μ), and Young's modulus (Y) for Ni and InAs. Experimental values are shown in brackets (Ref. [39] for InAs and Ref. [40] for Ni).

	InAs	Ni
a_0 [Å]	6.079 (6.058)	3.468 (3.508)
ρ [g/m^3]	5.61 (5.67)	9.35 (8.91)
B [GPa]	55.9 (58)	231.7 (186)
μ [GPa]	27.0 (19.0)	114.9 (76.0)
Y [GPa]	47.6 (51.5)	199.6 (200.0)

1. *Pmmn* (0.0 eV/f.u.)

2. *Pbcm* (0.010 eV/f.u.)

3. *P2₁/m* (0.017 eV/f.u.)

4. *Cmcm* (0.059 eV/f.u.)

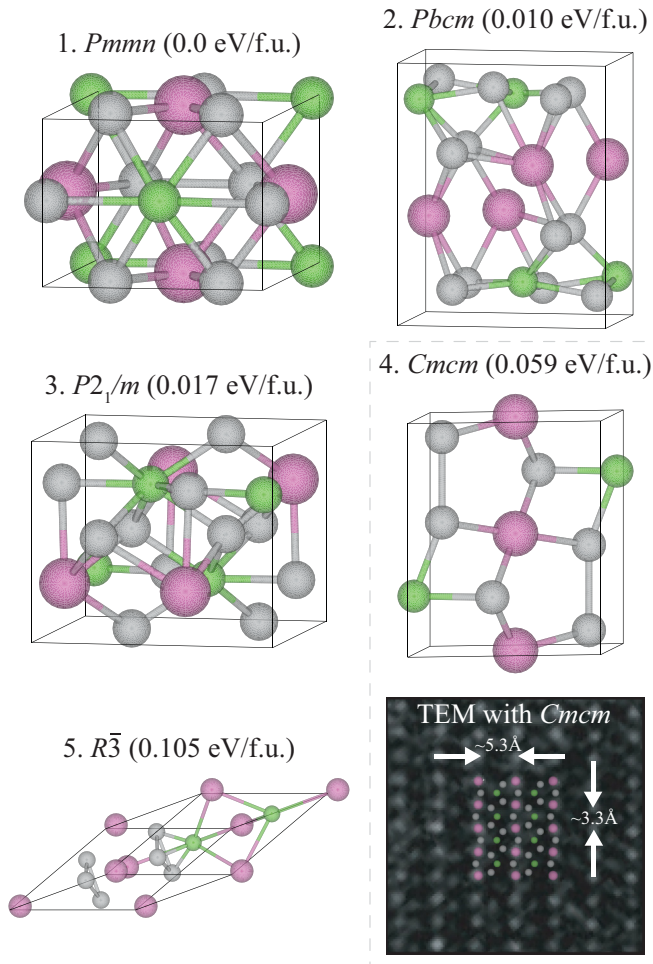5. *R3̄* (0.105 eV/f.u.)

TEM with *Cmcm*

~5.3Å

~3.3Å

FIG. 2. (Color online) Unit cell of the five lowest-energy Ni$_3$InAs structures labeled according to their space group. The relative energy of each structure with respect to the lowest-energy *Pmmn* structure is given in brackets. We also show the *Cmcm* structure overlaid on a zoomed-in image of the TEM results, which originally appeared in Ref. [5]. TEM image ©2012 IEEE. Reprinted, with permission, from Ref. [5]. Purple, green, and gray circles represent In, As, and Ni atoms, respectively.

in Fig. 1 slices through the ternary convex hull (solid lines) as well as the binary convex hull of Ni$_y$(InAs)$_{1-y}$ (dashed line). For the binary convex hull the compounds of Ni$_x$InAs with $x = 3,5$ are found to be stable with respect to Ni and InAs. We find that these low-energy structures for $x = 3,5$ lie approximately 0.01eV/atom above the ternary convex hull. This very small value indicates that the compounds for these two stoichiometries are only marginally unstable with respect to the known binary compounds and we expect these compounds to be found in experiments. The crystal structures for $x = 1,2,4,6$ are further above the convex hull, indicating that these phases are significantly less stable in comparison to $x = 3$ and 5 . We focus on $x = 3$ in this study, which is consistent with the growth procedure and layer thicknesses in Ref. [5] and the EDS results presented for the nanowires in Ref. [6]. We find five low-energy structures for $x = 3$, which we consider here in detail. The atomic structures are shown in Fig. 2 for the possible low-energy configurations [25],

TABLE II. Unit cell parameters of the Ni$_3$InAs low-energy structures.

space group	a [Å]	b [Å]	c [Å]	α[degree]	β[degree]	γ[degree]
Pmmn	4.99	3.76	7.20	90.00	90.00	90.00
Pbcm	6.56	8.22	5.01	90.00	90.00	90.00
P2₁/m	6.46	5.26	8.02	90.00	86.15	90.00
Cmcm	5.71	6.84	3.75	90.00	109.24	90.00
R3̄	7.23	7.23	7.23	40.29	40.29	40.29

with their lattice parameters in Table II. The structure with *Pmmn* space group has the lowest formation energy, followed in order of decreasing stability by the structures with space group *Pbcm*, *P2₁/m*, *Cmcm*, and *R3̄*. We show the associated relative energies for the higher-energy structures in brackets in Fig. 2. The energetic ordering of *Cmcm* Ni$_3$InAs is not significantly affected when other XC functionals are considered. In addition to PBEsol, we also consider three other common XC correlation functionals, LDA [34], PBE, and WC [35]. The results for the five low-energy structures of Ni$_3$InAs are compared in Table III. Although the exact energetic ordering changes slightly for the three lowest-energy structures, the energetic ordering of the *Cmcm* Ni$_3$InAs structure is not significantly affected: It always remains a higher-energy metastable structure.

We compare our crystal structures to the limited information available in the literature for the crystal structure of Ni$_3$InAs. By visual inspection, we find that the crystal structure of Ni$_x$InAs found in Ref. [5] is characterized by a lattice periodicity of approximately 5.3 Å by 3.3 Å (reproduced in Fig. 2). These dimensions were determined based on the known lattice constant of InAs shown in the original TEM in Ref. [5]. This is in excellent agreement with the periodicity of the *Cmcm* structure we find, which in its 4 f.u. orthorhombic representation has a unit cell size of 10.76 Å × 6.84 Å × 3.75 Å or $(2 \cdot 5.38)$ Å × $(2 \cdot 3.42)$ Å × 3.75 Å and $\alpha = \beta = \gamma = 90.0°$. Half the distances of the full lattice give the periodicity of the In atoms, consistent with the experiments in Ref [5], if projected on the plane. We overlay our *Cmcm* structure on the TEM image of Ref. [5] in Fig. 2. We overlap In, the heaviest of the three elements, with the brightest regions of the TEM. This comparison strongly suggests that the *Cmcm* structure is the structure that resulted from the silicidelike growth on InAs. The TEM images of Ref. [6] did not correspond to any of our low-energy structures. It is likely that the very different geometry in the nanowires resulted in a very different growth mechanism and hence different crystal structure.

Our computational results indicate that three phases lower in energy than the *Cmcm* structure observed in the experiments of Ref. [5] exist. There are several possible explanations why the higher-energy *Cmcm* structure may form: (i) First, it is possible that at the high temperatures during the anneal process, the *Cmcm* structure is energetically more favorable, and then becomes trapped in this higher-energy state. (ii) It may also be possible that the energy barrier to create the *Cmcm* structure from the InAs structure with interdiffused Ni is just significantly smaller than to any other phase. Annealing with higher temperatures may provide experimental evidence for

TABLE III. Energetic ordering of the five lowest-energy structures using the LDA, PBE, PBEsol, and WC XC functionals.

PBEsol		WC		PBE		LDA	
structure	ΔE (eV/f.u.)	structure	ΔE (eV/f.u.)	structure	ΔE (eV/f.u.)	structure	ΔE (eV/f.u.)
$Pmmn$	–	$Pmmn$	–	$P2_1/m$	–	$Pmmn$	–
$Pbcm$	0.010	$P2_1/m$	0.007	$Pmmn$	0.005	$P2_1/m$	0.006
$P2_1/m$	0.017	$Pbcm$	0.007	$Pbcm$	0.011	$Pbcm$	0.007
$Cmcm$	0.059	$Cmcm$	0.029	$Cmcm$	0.011	$Cmcm$	0.033
$R\bar{3}$	0.105	$R\bar{3}$	0.096	$R\bar{3}$	0.062	$R\bar{3}$	0.102

the latter. (iii) Alternatively, it is possible that the interface structure to InAs plays an important role. We find that of all five low-energy structures, the least strained interface can be formed with the $Cmcm$ structure. All these considerations may have important implications for the usage of Ni_3InAs in transistor devices and warrant further investigation that are now possible since the crystal structures have been determined.

By considering the electronic density of states (DOS) of the five lowest-energy structures, we find that all are metallic (see Fig. 3), confirming what was suggested in the previous experimental work. Calculations of the DOS of $Cmcm$ Ni_3InAs using the hybrid HSE06 functional [26,27] further confirm the metallic nature of this compound: We again find a nonzero value of the density of states at the Fermi level (Fig. 4), confirming the results based on the GGA functional shown in Fig. 3. We also show in Fig. 5 the partial density of states (PDOS) of $Cmcm$ Ni_3InAs. We perform spin-polarized calculations to assess the magnetic properties and find that all five structures are nonmagnetic. We further investigate the mechanical properties of the five structures. The bulk, shear, and Young's moduli are summarized in Table IV and it can be seen that they are very similar for the four lowest-energy structures, while there are distinct differences in comparison to the $R\bar{3}$ structure. We calculate the elastic constants of the five low-energy structures and find them all to be mechanically

stable [28]. The values of B, μ, and Y for all Ni_3InAs structures lie approximately halfway between those of Ni and InAs. More details on the mechanical properties can be found in Appendix A.

Since the nickelide is intended as a contact material to InAs, it is important, beyond it being metallic, to assess the type of electronic barrier that forms between Ni_3InAs and InAs. We first consider the work function of Ni_3InAs in its $Cmcm$ crystal structure and find that for the (010) plane, which is the same geometry as for the interface in the experiments of Ref. [5], the work function is between $\Phi = 3.96$–4.40 eV (see Table V). The lower and higher values are for In- and As/Ni-terminated surfaces, respectively. The work functions for the (100) and (001) planes are similar in magnitude. In the traditional Schottky-Mott model, this can be compared to the electron affinity of InAs, which is experimentally known to be $\chi = 4.9$ eV [37]. For $\Phi < \chi$, as in our case here, the model then predicts Ohmic behavior for the interface.

It is well known that the Schottky-Mott band alignment model often fails to predict the correct interface behavior [29]. We therefore further perform calculations of the interface to determine the Schottky barrier height directly [30–32]. Our interface structure is based on the experimental TEM images of Oxland *et al.* [5]. We match the Ni_3InAs and InAs regions such that the standard {110} and {101} InAs[001] surface vectors are aligned with the {100} and {010} Ni_3InAs[001] surface vectors. A small section of the atomic structure is shown in Fig. 6. Although, of the five lowest-energy structures, the
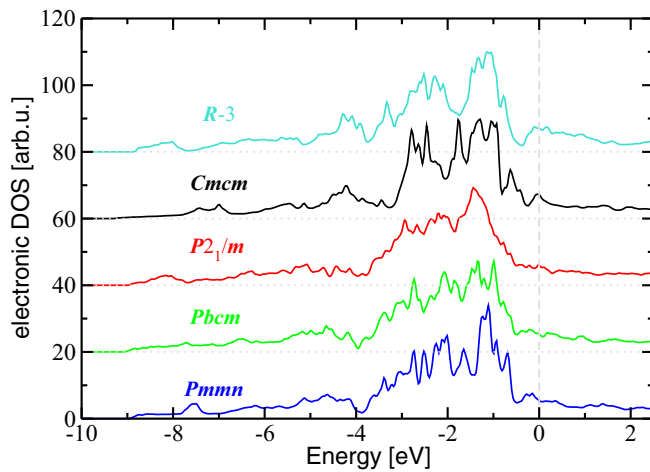

FIG. 3. (Color online) Electronic density of states of the five lowest-energy structures of Ni_3InAs. All structures are found to have a nonzero value of the density of states at the Fermi level, showing their metallic nature. The Fermi energy is shown as a dashed gray vertical line. Gray dotted horizontal lines indicate the zero offset of the shifted curves.
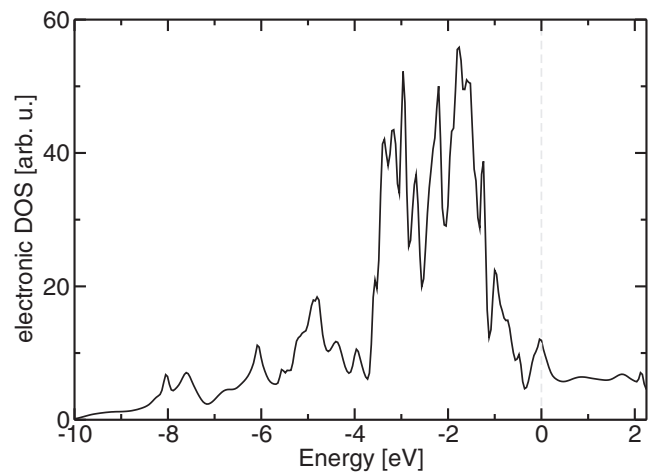

FIG. 4. Density of states of $Cmcm$ Ni_3InAs. The calculations were performed using the hybrid HSE functional and show metallic behavior further validating the results shown in Fig. 3.
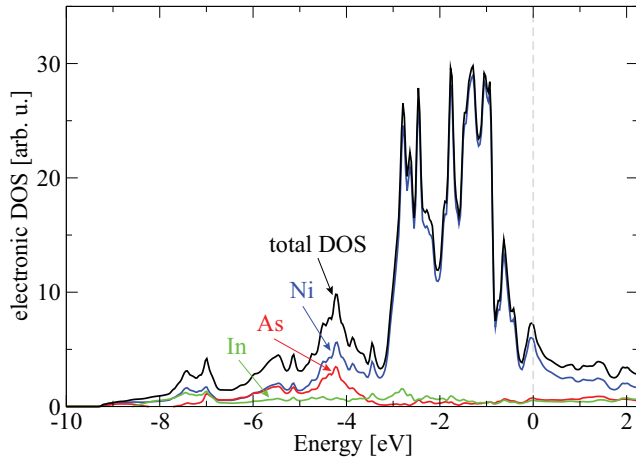
FIG. 5. (Color online) Partial density of states of *Cmcm* Ni$_3$InAs. The calculations show that the metallic behavior shown in Fig. 3 can be traced back to the Nickel atoms.

Cmcm structure matches the InAs structure best, the matching conditions nevertheless require 2×8 unit cells of Ni$_3$InAs matched with 5×7 lattice repeat units of InAs or an interface with extension of approximately 30.1 Å $\times$ 21.5 Å. This then results in a strain in the plane of the interface of less than 0.13% and 0.30%, respectively. Cells with 6.5 bilayers of InAs and two unit cells of Ni$_3$InAs perpendicular to the interface are studied. Due to the large system sizes involved we perform the majority of our calculations only using the ideal fixed structures as a first approximation. We consider In-terminated Ni$_3$InAs structures matched to As-terminated InAs with a total of 1127 atoms in the cell.

To account for the deficiencies of semilocal exchange correlation functionals in DFT to accurately describe band gaps and band alignment, we here use an approach combining the hybrid HSE functional [26,27] with results from conventional semilocal calculations [33] in studying the Schottky barrier [30]. This relies on calculating the local electrostatic potential of the interface using PBE as a reference for band alignment, while using HSE to determine the band gap of InAs and the band alignment of bulk Ni and InAs with respect to the local potential (further details on the interface calculations can be found in Appendix B). We find an *n*-type Schottky barrier height of -0.55 eV, suggesting that the interface is Ohmic, with the Fermi level found lying in the conduction band of InAs. This behavior has been checked to be independent of the cell sizes used. To assess the influence of Ni diffusion

into the bulk InAs region, we further calculate the Schottky barrier height for a structure with two sheets of interstitials inserted into the InAs region adjacent to the interface with a density of 1.85×10^{14}/cm^2. This is a likely defect to occur at the InAs/Ni3InAs interface, since Ni$_3$InAs is expected to grow via Ni diffusion into InAs during anneal. Such additional Ni interstitials added to the InAs region only further increase the offset of the Fermi level with respect to the conduction band and result in a Schottky barrier height of -0.99 eV.

IV. CONCLUSIONS

In summary, we have studied the ternary compounds formed by Ni, In, and As and whether they could function as viable candidates for contacts to InAs. Investigating the
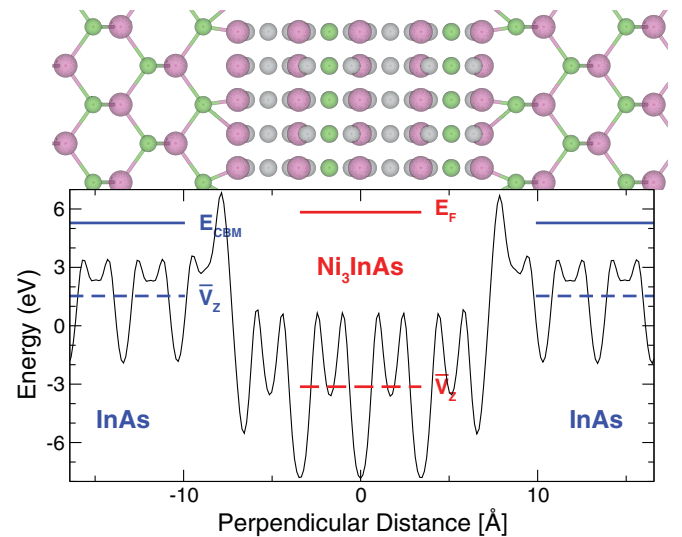
TABLE V. Work function, Φ, and electron affinity, χ, for Ni, InAs, and Ni$_3$InAs in its *Cmcm* structure. The cleavage planes are defined based on the orthorhombic *Cmcm* structure with 4 f.u., which has lattice constants $a = 10.76$ Å, $b = 6.84$ Å, $c = 3.75$ Å, and angles $\alpha = \beta = \gamma = 90.0°$. Numbers in brackets are experimental results from [a] Ref. [37] and [b] Ref. [38].

	Φ [eV]	χ [eV]
InAs (100)	–	4.53 (4.9)[a]
Ni (100)	4.99 (5.01)[b]	–
Ni$_3$InAs *Cmcm* (010)	3.96–4.40	–
Ni$_3$InAs *Cmcm* (100)	4.39–4.79	–
Ni$_3$InAs *Cmcm* (001)	4.76	–

FIG. 6. (Color online) Atomic structure of the InAs/Ni$_3$InAs interface and the planar averaged electrostatic local reference potential, $\bar{V}$, as a function of the perpendicular distance from the interface. The macroscopic average of the local reference potential is shown as dashed red and blue lines in the Ni$_3$InAs and InAs regions, respectively. The Fermi energy of the Ni$_3$InAs region is shown as a red solid line, while the conduction band minimum (CBM) of the InAs region is shown as a blue line. Only a small section of the total atomic structure of the interface is shown. Purple, green, and gray circles represent In, As, and Ni atoms, respectively.

TABLE IV. Density ρ, bulk modulus B, shear modulus, μ, and Young's modulus, Y of the five lowest-energy structures of Ni$_3$InAs.

	ρ [g/cm^3]	B [GPa]	μ [GPa]	Y [GPa]		
				x	y	z
Pmmn	8.99	157.1	58.68	200.2	151.5	158.1
Pbcm	9.00	161.2	48.1	182.0	177.6	174.5
P2$_1$/m	8.93	152.5	58.2	146.7	165.3	150.5
Cmcm	8.79	158.7	64.0	139.7	192.4	132.1
R$\bar{3}$	8.54	209.5	42.5	190.6	190.6	109.4

physical properties of the ternary nickelides using computational methods crucially relies on finding the crystal structure first: We have employed the *ab initio* random structure searching approach to find the low-energy phases and were able to identify the structure formed in the experiments of Ref. [5]. This ternary nickelide with orthorhombic crystal structure and *Cmcm* space group is found to be both metallic and forms Ohmic contacts to InAs. This makes the material a viable candidate for contacts in next-generation InAs-based MOS. However, further investigations to better understand long-term stability are warranted, since our results indicate that the structure formed in experiments is not in fact predicted to be the lowest-energy structure in DFT. We illustrate how, in general, with minimal experimental input a complete theoretical assessment of new materials can be performed computationally, all the way from finding the crystal structure to its stability and properties and even interactions with other materials to study device behavior and assess their functionality. This may have important implications for especially the high-technology industry, where technological materials advantages have until now often come in the form of expensive experiments with the detailed results often withheld from competitors and the public. Cheap computational approaches may provide disruptive technologies and, beyond its predictive powers, this approach may also enable computational reverse engineering and thereby help in leveling the playing field in the high-technology industry. The approach outlined here will undoubtedly find more applications for technologies of great industrial importance.

APPENDIX A: ADDITIONAL MECHANICAL PROPERTIES

We show in Table VI the elastic constants of the five lowest-energy structures of Ni_3InAs and find that all structures are structurally stable based on the standard stability criteria for the elastic constants [28].

TABLE VI. The elastic constants for the five low-energy structures of Ni_3InAs. All structures are found to be mechanically stable based on the stability conditions for the elastic constants [28].

	Pmmn	Pbcm	P2$_1$/m	Cmcm	R$\bar{3}$
C_{11} [GPa]	258.3	262.8	227.3	209.0	361.9
C_{22} [GPa]	236.1	243.9	236.9	288.0	361.9
C_{33} [GPa]	240.7	248.8	227.5	220.0	208.9
C_{44} [GPa]	68.3	31.6	57.1	93.1	22.7
C_{55} [GPa]	41.3	63.7	51.8	51.2	22.7
C_{66} [GPa]	59.2	28.0	67.33	68.1	82.5
C_{12} [GPa]	106.0	115.2	112.2	112.9	197.0
C_{13} [GPa]	101.3	124.3	118.6	115.8	167.0
C_{14} [GPa]	–	–	–	–	−14.3
C_{15} [GPa]	–	–	9.9	–	−7.9
C_{23} [GPa]	132.4	109.4	110.0	136.0	167.0
C_{24} [GPa]	–	–	–	–	14.3
C_{25} [GPa]	–	–	−1.0	–	7.9
C_{35} [GPa]	–	–	−2.0	–	–
C_{46} [GPa]	–	–	−0.9	–	7.9
C_{56} [GPa]	–	–	–	–	−14.3

APPENDIX B: INTERFACE CALCULATIONS

To assess our computational approximations for the 1127 atom interface structure we perform comparison calculations on a second structure: A $1 \times 1 \times 8$ supercell of InAs with an eight-atom cubic cell ($6.15\,\text{Å} \times 6.15\,\text{Å} \times 6.15\,\text{Å}$) was generated, with half of the structure being populated with Ni interstitials introduced such that the stoichiometry of the cell is $Ni(InAs)_2$/InAs. We relax this structure such that the resultant forces were smaller than $0.01\,\text{eV/Å}$ and compare it to the unrelaxed ideal structure. We find that the change in the local reference potential across the interface changes by less than 0.1 eV when relaxations are considered; a value significantly smaller than the magnitude of the Schottky barrier height we find, and hence negligible in determining that the interface is Ohmic in character. We also examine the effects of varying the energy cutoff between 270 eV and 350 eV and found no change in the behavior of the local reference potential, $\Delta \bar{V}$, at the interface for either supercell. Finally, to further validate the approach used here, we calculate $\Delta \bar{V}$ for this system using HSE and PBE and find the difference between the results to be less than 0.05 eV. This is in agreement with Ref. [30], showing that the local potential alignment is not critically affected by the choice of the functional. This last result may be of use to many performing band alignment calculations.

[1] International Technology Roadmap for Semiconductors (2013); http://www.itrs.net

[2] Jesús A. del Alamo, Nature (London) **479**, 317 (2011).

[3] Hyunhyub Ko, Kuniharu Takei, Rehan Kapadia, Steven Chuang, Hui Fang, Paul W. Leu, Kartik Ganapathi, Elena Plis, Ha Sul Kim, Szu-Ying Chen, Morten Madsen, Alexandra C. Ford, Yu-Lun Chueh, Sanjay Krishna, Sayeef Salahuddin, and Ali Javey, Nature (London) **468**, 286 (2010).

[4] S. W. Chang, Xu Li, R. Oxland, S. W. Wang, C. H. Wang, R. Contreras-Guerrero, K. K. Bhuwalka, G. Doornbos, T. Vasen, M. C. Holland, G. Vellianitis, M. J. H. van Dal, B. Duriez, M. Edirisooriya, J. S Rojas-Ramirez, P. Ramvall, S. Thoms, U. Peralagu, C. H. Hsieh, Y. S. Chang, K. M. Yin, E. Lind, L.-E. Wernersson, R. Droopad, I. Thayne, M. Passlack, and C. H. Diaz, in *Proceedings of the IEEE International Electron Devices Meeting (IEDM)* (IEEE, Piscataway, NJ, 2013), pp. 16.1.1–16.1.4.

[5] R. Oxland, S. W. Chang, Xu Li, S. W. Wang, G. Radhakrishnan, W. Priyantha, M. J. H. van Dal, C. H. Hsieh, G. Vellianitis, G. Doornbos, K. Bhuwalka, B. Duriez, I. Thayne, R. Droopad,

M. Passlack, C. H. Diaz, and Y. C. Sun, IEEE Electron Device Lett. **33**, 501 (2012).

[6] Yu-Lun Chueh, Alexandra C. Ford, Johnny C. Ho, Zachery A. Jacobson, Zhiyong Fan, Chih-Yen Chen, Li-Jen Chou, and Ali Javey, Nano Lett. **8**, 4528 (2008).

[7] D. Swenson and Y. A. Chang, Mater. Sci. Eng. B **39**, 232 (1996).

[8] Szu-Ying Chen, Chiu-Yen Wang, Alexandra C. Ford, Jen-Chun Chou, Yi-Chung Wang, Feng-Yun Wang, Johnny C. Ho, Hsiang-Chen Wang, Ali Javey, Jon-Yiew Gan, Lih-Juann Chen, and Yu-Lun Chueh, Phys. Chem. Chem. Phys. **15**, 2654 (2013).

[9] Chin-Hung Liu, Szu-Ying Chen, Cheng-Ying Chen, Jr-Hau He, Lih-Juann Chen, Johnny C. Ho, and Yu-Lun Chueh, ACS Nano **5**, 6637 (2011).

[10] C. J. Pickard and R. J. Needs, Phys. Rev. Lett. **97**, 045504 (2006).

[11] C. J. Pickard and R. J. Needs, Nature Mater. **9**, 624 (2010).

[12] C. J. Pickard and R. J. Needs, Nature Mater. **7**, 775 (2008).

[13] C. J. Pickard and R. J. Needs, Nature Phys. **3**, 473 (2007).

[14] Jian Sun, Miguel Martinez-Canales, Dennis D. Klug, Chris J. Pickard, and Richard J. Needs, Phys. Rev. Lett. **108**, 045503 (2012).

[15] A. J. Morris, R. J. Needs, E. Salager, C. P. Grey, and C. J. Pickard, Phys. Rev. B **87**, 174108 (2013).

[16] A. J. Morris, Chris J. Pickard, and R. J. Needs, Phys. Rev. B **80**, 144112 (2009).

[17] A. J. Morris, C. J. Pickard, and R. J. Needs, Phys. Rev. B **78**, 184102 (2008).

[18] G. Schusteritsch and C. J. Pickard, Phys. Rev. B **90**, 035424 (2014).

[19] Steward J. Clark, Matthew D. Segall, Chris J. Pickard, Phil J. Hasnip, Matt I. J. Probert, Keith Refson, and Mike C. Payne, Z. Kristallogr. **220**, 567 (2005).

[20] John P. Perdew, Adrienn Ruzsinszky, Gábor I. Csonka, Oleg A. Vydrov, Gustavo E. Scuseria, Lucian A. Constantin, Xiaolan Zhou, and Kieron Burke, Phys. Rev. Lett. **100**, 136406 (2008).

[21] Philipp Haas, Fabien Tran, and Peter Blaha, Phys. Rev. B **79**, 085104 (2009).

[22] G. Kresse and J. Furthmüller, Phys. Rev. B **54**, 11169 (1996).

[23] P. E. Blöchl, Phys. Rev. B **50**, 17953 (1994).

[24] G. Kresse and D. Joubert, Phys. Rev. B **59**, 1758 (1999).

[25] See Supplemental Material at http://link.aps.org/supplemental/10.1103/PhysRevB.92.054105 for the atomic coordinates as *cif* files of all structures.

[26] J. Heyd, G. E. Scuseria, and M. Ernzerhof, J. Chem. Phys. **124**, 219906 (2006).

[27] J. Heyd, G. E. Scuseria, and M. Ernzerhof, J. Chem. Phys. **118**, 8207 (2003).

[28] R. A. Cowley, Phys. Rev. B **13**, 4877 (1976).

[29] Raymond T. Tung, Applied Phys. Rev. **1**, 011304 (2014).

[30] Karim Steiner, Wei Chen, and Alfredo Pasquarello, Phys. Rev. B **89**, 205309 (2014).

[31] K. T. Delaney, N. A. Spaldin, and C. G. Van de Walle, Phys. Rev. B **81**, 165312 (2010).

[32] A. Baldereschi, S. Baroni, and R. Resta, Phys. Rev. Lett. **61**, 734 (1988).

[33] J. P. Perdew, K. Burke, and M. Ernzerhof, Phys. Rev. Lett. **77**, 3865 (1996).

[34] J. P. Perdew and A. Zunger, Phys. Rev. B **23**, 5048 (1981).

[35] Z. Wu and R. E. Cohen, Phys. Rev. B **73**, 235116 (2006).

[36] STOOLS toolset, https://github.com/muhrin/STools.

[37] P. Bhattacharya, *Semiconductor Optoelectronic Devices* (Prentice-Hall, Upper Saddle River, 1997).

[38] P. A. Tipler and R. A. Llewellyn, *Modern Physics* (W. H. Freeman and Company, New York, 2008).

[39] Sadao Adachi, *Handbook on Physical Properties of Semiconductors* (Kluwer Academic Publishers, Boston, 2004), Vol. 2.

[40] D. R. Lide (ed.), *CRC Handbook of Chemistry and Physics*, 95th ed. (CRC Press, Boca Raton, 2014); G. W. C. Kaye and T. H. Laby, *Tables of Physical and Chemical Constants*, 16th ed. (Longman, London, 1995); C. Kittel, *Introduction to Solid State Physics* (John Wiley & Sons, Hoboken, 1996).